Journal of Molecular Graphics and Modelling 106 (2021) 107933

Contents lists available at ScienceDirect

Journal of Molecular Graphics and Modelling

journal homepage: www.elsevier.com/locate/jmgm

Rational design, chemical synthesis and cellular evaluation of novel 1,3-diynyl derivatives of noscapine as potent tubulin binding anticancer agents

Amiya Kumar Patel [a], Rajesh Kumar Meher [a], Praveen Kumar Reddy [b], Ravi Kumar Pedapati [b], Pratyush Pragyandipta [a], Srinivas Kantevari [b], Manas Ranjan Naik [c], Pradeep Kumar Naik [a,*]

[a] Centre of Excellence in Natural Products and Therapeutics, Department of Biotechnology and Bioinformatics, Sambalpur University, Jyoti Vihar, Burla, Sambalpur-768019, Odisha, India
[b] Fluoro and Agrochemicals Division, CSIR-Indian Institute of Chemical Technology, Hyderabad 500 007, India
[c] Department of Pharmacology, SLN Medical College, Koraput-764020, Odisha, India

ARTICLE INFO

Keywords:
Noscapine
1, 3-Diynyl-noscapinoids
Tubulin binding
Anticancer agents
Breast cancer

ABSTRACT

We present a new class of derivatives of noscapine, 1,3-diynyl-noscapinoids of an antitussive plant alkaloid, noscapine based on our *in silico* efforts that binds tubulin and displays anticancer activity against a panel of breast cancer cells. Structure-activity analyses pointed the C-9 position of the isoquinoline ring which was modified by coupling of 1,3-diynyl structural motifs to rationally design and screened a series of novel 1,3-diynyl-noscapinoids (**20–22**) with robust binding affinity with tubulin. The selected 1,3-diynyl-noscapinoids, **20–22** revealed improved predicted binding energy of −6.568 kcal/mol for **20**, -7.367 kcal/mol for **21** and -7.922 kcal/mol for **22**, respectively in comparison to the lead molecule (−5.246 kcal/mol). These novel derivatives were chemically synthesized and validated their anticancer activity based on cellular studies using two human breast adenocarcinoma, MCF-7 and MDAMB-231, as well as with a panel of primary breast cancer cells isolated from patients. Interestingly, all these derivatives inhibited cellular proliferation in all the cancer cells that ranged between 6.2 to 38.9 μM, which is 6.7 to 1.5 fold lower than that of noscapine. Unlike previously reported derivatives of noscapine that arrests cells in the S-phase, these novel derivatives effectively inhibit proliferation of cancer cells, arrests cell cycle in the G2/M-phase followed by apoptosis and appearance of apoptotic cells. Thus, we conclude that 1,3-diynyl-noscapinoids have great potential to be a novel therapeutic agent for breast cancers.

1. Introduction

Currently available breast cancer chemotherapeutic regimens have been encumbered by poor selectivity because most antiproliferative drugs are toxic not only to tumor cells but also to body's non-neoplastic cells [1–5]. This unsatisfactory situation has driven intensive research over the last few decades towards more specific and less toxic anticancer drugs. Noscapine, a safe anti-tussive agent, is an excellent choice of drug to use however, because of the nature of its action; it is not harmful to healthy cells [6,7]. It is also well tolerated in humans and has been shown to be non-toxic in healthy volunteers including pregnant mothers [8–10]. Noscapine, has been discovered as a novel selective tubulin-binding anticancer drug that does not change the steady state monomer/polymer ratio of tubulin over a wide range of concentrations. This is a unique edge over currently-available antimicrotubule drugs that either inhibit microtubule disassembly (taxanes, epothilone) or inhibit tubulin assembly (vincas, eribulin, estramustine, drug-antibody complexes with dolastatin 10 and maytansine analogs) and hence cause various debilitating toxicities such as leucocytopenias, diarrhea, alopecia and peripheral neuropathies [4,5,11]. Owing to absence of extreme effects on microtubules, noscapine does not cause any hemo-, immuno- and neuronal toxicity. The basis for not killing healthy cells seems to be that noscapine subtly attenuates microtubule dynamics just enough to activate the mitotic checkpoints in normal cells, and halts their cell-cycle reversibly until the drug is cleared by metabolism and excretion [12]. Whereas, cancer cells upon noscapine treatment do not halt for long durations due to mutational lesions in their checkpoint mechanisms; instead they continue to traverse the cell-cycle without cell

* Corresponding author.
E-mail addresses: pknaik1973@gmail.com, pknaik1973@suniv.ac.in (P.K. Naik).

https://doi.org/10.1016/j.jmgm.2021.107933
Received 14 November 2020; Received in revised form 29 March 2021; Accepted 19 April 2021
Available online 5 May 2021

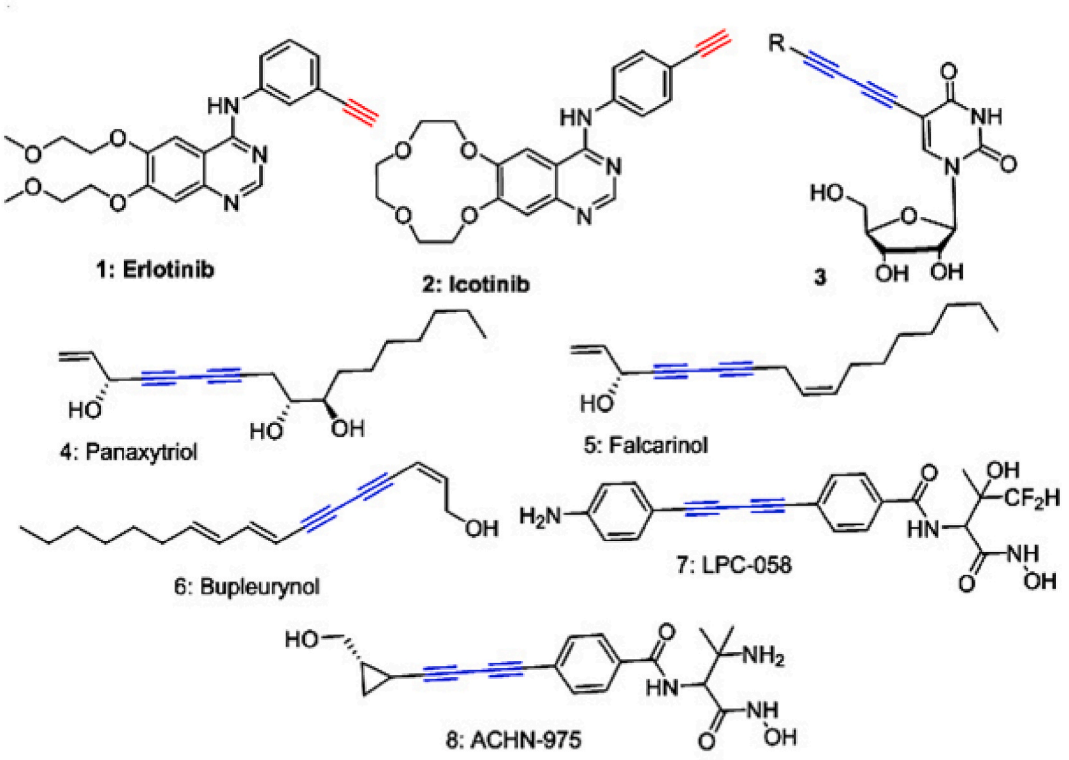

Fig. 1. Structures of anticancer drugs **1** and **2** containing ethyne group and 1,3-diyne containing bioactive natural and synthetic products **3–8**.

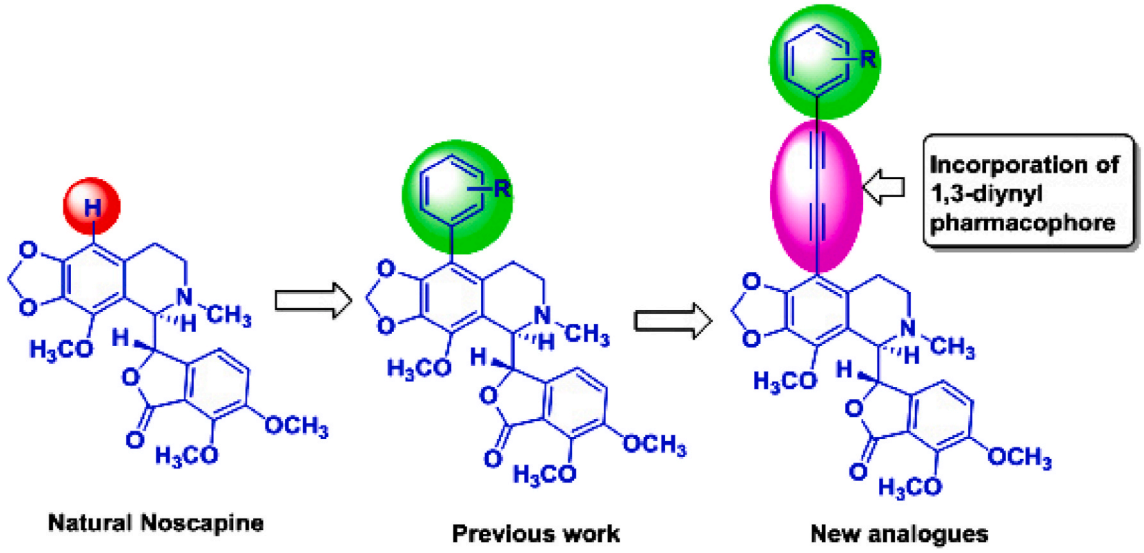

Fig. 2. Rational design of novel 1,3-diynyl noscapinoids. A library of 1,3-dinyl congeners of noscapine were developed by derivatization at C-9 position of the scaffold of noscapine.

division, thus accumulating genotoxic DNA amounts that trigger apoptosis [13]. It is previously reported that noscapine retains activity against paclitaxel-resistant ovarian cancer [14] has favorable pharmacokinetics (clearance in 6–10 h [8], is a poor substrate for drug-efflux pumps (polyglycoportiens and MDR-related proteins) [7] that comprise a major cause of drug resistance; does not show immunological [15,16] and neurological toxicities [17]. The only drawback of noscapine is that it requires relative high concentration of 25–250 μM *in vitro* to induce apoptotic cell death to tumor cells [6]. Although noscapine can inhibit tumor growth and cause regression of localized breast tumor xenografts to a fair degree of extent in preclinical mice models, a complete obliteration of the disease has not been achieved even on increasing noscapine dosage as high as 600 mg/kg [6]. Therefore, more potent derivative of noscapine will be required for the effective treatment of breast cancer. We have already developed a battery of noscapinoids, some of which have shown 40–80 folds more potent compared to noscapine as anticancer compounds [18–23]. Most importantly, 9-bromonoscapine was patented [24] and introduced into clinical trials against non-Hodgkin's lymphoma and chronic lymphocytic leukemia. Several other 9-substituted noscapine derivatives were reported recently [14,19,21,23]. For instance 9-nitronoscapine was found to be active against drug-resistant ovarian cancer and T-cell lymphoma cells [14],

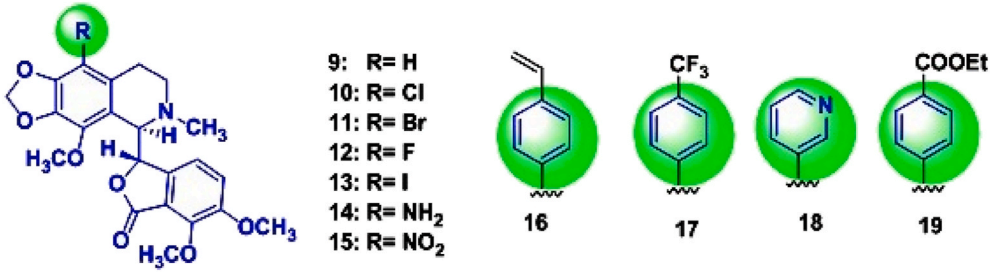

Fig. 3. Molecular structures of previously reported noscapine derivatives that have experimentally proven to bind tubulin with known binding free energy (Table 1) and used as training set molecules for LIE-SGB model building.

and its reduced congener, 9-aminonoscapine [23], as well as biaryl inserted noscapine analogs [19] have good activity as a tubulin binding anticancer agents.

Considering the increased activity of 9′-substituted derivatives compared to its parent molecule, noscapine, in this study, we approach to develop a new series of noscapine derivatives by substituting 1,3-dinyl functional group at the C9′-position (called diyne derivatives) based on our *in silico* efforts. These derivatives were then chemically synthesized and validated their anticancer activity based on cellular study using two established human breast cancer cell lines, MCF-7 and MDAMB-231, as well as a panel of primary breast cancer cells obtained from the patients. The novel derivatives were found to bind tubulin heterodimer with increased binding affinity, effectively inhibit cancer cell proliferation and causes selective G2/M arrest in cancer cells. The mitotic catastrophe in cancer cells is then followed by induction of apoptosis.

2. Materials and methods

2.1. Protein preparation

The co-crystallized PDB structure of the amino noscapine-tubulin complex (PDB ID: 6Y6D, resolution 2.20 Å) [25] was used for the molecular docking and calculation of binding affinity of the noscapinoids. The structure was refined by molecular mechanics energy minimization using OPLS 2005 force field with Polak-Ribiere Conjugate Gradient (PRCG) algorithm (energy gradient of 0.001 kcal/mol) using Macromodel (Schrödinger). Moreover, it was further refined by performing an all atom molecular dynamics (MD) simulation of 100 ns in explicit water using GROMACS 4.5.4 software [27] and the GROMOS96 force field with similar parameters set up as reported earlier [26]. A time step of 2 fs was used for sampling from the MD trajectory, whereas the top most 5 structures of the Tubulin based on the lowest minimum total energy from the MD trajectory were used to generate an average structure of the tubulin.

2.2. Rational design of 1,3-diynyl derivatives of noscapine

In pursuance of our efforts to develop potential derivatives of the lead molecule, noscapine, we have designed a new series of its derivatives by coupling of ethyne and 1,3-diynes functionality with the scaffold. It is because several natural products **1–8** (Fig. 1) which are in the clinics consists of ethyne and 1,3-diynes functionality as active pharmacophore for their anticancer, anti-HIV, antifungal, antibacterial and antiviral activities [28–37]. Initially we have developed a library of 1,3-diyne derivatives of noscapine by various substitutions as depicted in Fig. 2 by *in silico* combinatorial approach. These derivatives were then virtually screened using a combination of molecular docking and linear interaction energy model (LIE) with a surface generalized Born (SGB) continuum solvation model to determine predictive binding affinity and to obtain a panel of most potent derivatives. Further, the selected derivatives, co-complexed with tubulin were used to performed a molecular dynamics simulation of 100 ns followed by Molecular Mechanics Poisson-Boltzmann Surface Area (MM-PBSA) calculation to determine their predictive binding energy with tubulin. Moreover, the absorption, distribution, metabolism, and excretion (ADME) properties of these designed compounds were computationally evaluated using Qikprop (Schrodinger package) and were compared with the recommended values.

2.3. Preparation of molecular structure

Molecular structures of noscapinoids (Fig. 3) and newly designed 1,3-diynyl-noscapinoids (Fig. 2) were built using ChemDraw and were imported into Maestro (Schrödinger package). All these structures were energy minimized using Macromodel (Schrödinger package) and OPLS 2005 force field with PRCG algorithm (energy gradient of 0.001). Ligprep (Schrödinger package) was used to define appropriate bond order for each structure. The ligand structures were further refined using geometric optimization using Jaguar (Schrödinger, package). Hybrid density functional theory with Becke's three-parameter exchange potential and the Lee-Yang-Parr correlation functional (B3LYP) with basis set 3-21G* was used for the geometric optimization.

2.4. Molecular docking

Noscapinoids prepared above were docked onto the binding pocket at the interface of αβ-tubulin [25,38] using Glide docking (Schrödinger package). The binding pocket was fixed by defining two grid box using Glide grid generation program (Schrodinger package). In brief, an inner grid box of size 12 Å × 12 Å x 12 Å was defined at the centroid of the binding pocket by selecting the co-complex ligand, amino-noscapine in the crystal structure of tubulin (PDB ID: 6Y6D). This box defines the search space in which the diameter midpoint of each docked ligand is required to be present. Further, an outer grid box was also defined with a size of ≤24 Å of the co-complexed ligand, amino noscapine in the crystal structure. It defines the volume within which all ligand atoms of a valid pose must be located. All the noscapinoids were docked using Glide XP (extra precision) and evaluated using a Glide XP_{Score} function [39,40]. A scale factor of 0.4 for van der Waals radii was applied to atoms of protein with absolute partial charges less than or equal to 0.25. The single best conformation for each ligand was considered for further analysis.

2.5. LIE-SGB model building

A more accurate predictive model for predicting the binding free energy ($\Delta G_{bind,pred}$) of the newly designed 1,3-diynyl-noscapinoids with tubulin was developed based on linear interaction energy model (LIE) with a surface generalized Born (SGB) continuum solvation model [41]. A training data set of noscapinoids (Fig. 3) with known experimental binding free energy, $\Delta G_{bind,expt}$ was used and mapped with various predicted energy parameters such as van der Waals (U_{vdw}), coulumbic (U_{coul}), reaction field (U_{rxn}) and cavity energy (U_{cav}) based on LIE model to develop the empirical prediction model. Liaison programme

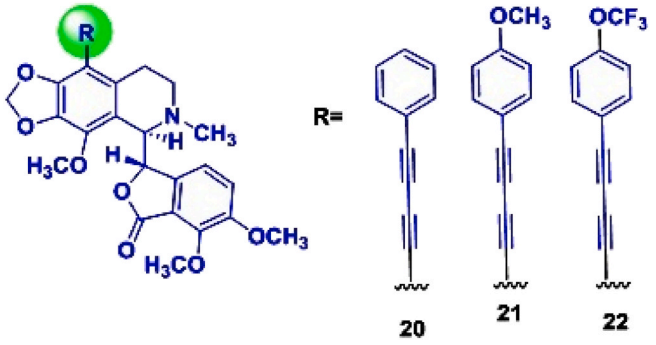

Fig. 4. Panel of the 1,3-diynyl derivatives of noscapine, **20–22** that were screened out with higher binding affinity compared to noscapine based on docking score and predictive binding free energy using LIE-SGB model.

(Schrödinger package) was used to estimate the above energy parameters from the docked complexes of the tubulin-noscapinoids based on Hybrid Monte Carlo simulation technique as reported previously [19]. A residue-based cut off of 12 Å was set for the non-bonding interactions.

$$\Delta G_{bind,pred} = \alpha\left(U^{b}_{vdw} - U^{f}_{vdw}\right) + \beta\left(U^{b}_{coul} - U^{f}_{coul}\right) + \gamma\left(U^{b}_{rxn} - U^{f}_{rxn}\right) + \delta\left(U^{b}_{cav} - U^{f}_{cav}\right)$$

Here⟨⟩represents the ensemble average, *b* represents the bound form of the ligand, *f* represents the free form of the ligand, and α, β, γ and δ are the coefficients determined using Minitab statistical package (Minitab Inc.) by fitting the experimental binding affinities of training set molecules. The $\Delta G_{bind,expt}$ for the reported noscapinoids was calculated from their respective dissociation constant (K_d) values using the relation:

$$\Delta G_{bind,expt} = RT \ln K_d$$

where R is gaseous constant (0.001986 kcal/mol) and T is temperature (298 K). The K_d values of the noscapinoids used in training set were obtained from earlier published work [14,19,21,23,42]. Finally based on the docking score and the predictive binding affinity using LIE-SGB model, we have screened out the following three 1,3-diynyl-noscapinoids (Fig. 4) having enhanced binding affinity with tubulin compared to noscapine for chemical synthesis and cellular evaluation to determine their anticancer potential.

2.6. Molecular dynamics simulation

Molecular dynamics (MD) simulation of 100 ns was performed using Amber 16 suite [29] for the docked complexes of tubulin and 1,3-diynyl noscapinoids, **20–22.** The ligands parameters were defined using Antechamber program of Amber 16 suite [30] and all atomic point charges were calculated using AM1-BCC charge model [31]. Topologies and internal coordinates of the complex were generated using tleap program in Amber16. The molecular system was neutralized by adding counter-ions and solvation using TIP3P water model in a truncated octahedron. The molecular system was relaxed and the bad contacts were removed by performing three rounds of minimization. Position restraints of 10 kcal/Å^2 and 2 kcal/Å^2 were imposed on the protein system for the first and the second round respectively, whereas no restraints were imposed in the third round. The molecular systems were equilibrated at 300 K and 1 atm for 500 ps. The equilibrated systems were then run for 100 ns each with time step of 2 fm. Throughout simulations, the cut-off for non-bonded interaction was 10 Å, electrostatics were calculated using Particle Mesh Ewald (PME) and bonds were constrained using shake algorithm [33–35]. Langevin thermostat was used to regulate the temperature of simulations. Co-ordinates were written every 20

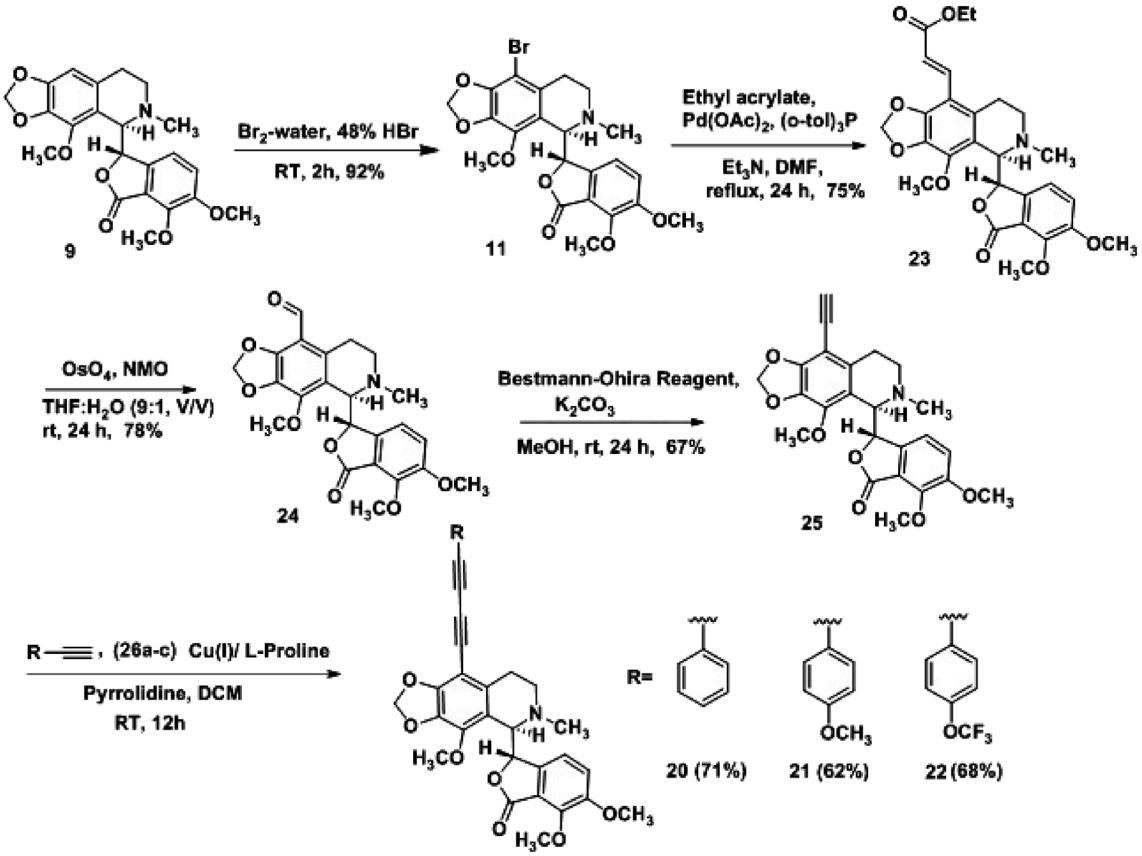

Fig. 5. Synthesis of 9-(1,3-diynyl) noscapinoids **20, 21** and **22** that have been rationally designed in the study. The percentage value mentioned within the bracket are the yield percentage.

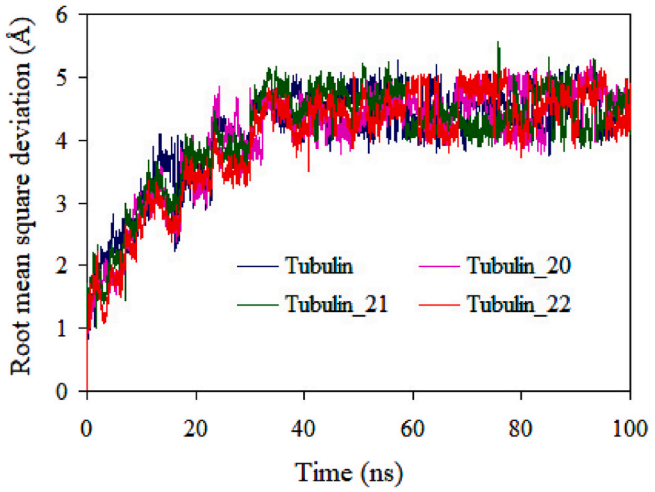

Fig. 6. Root mean square deviations (RMSD) of backbone Cα carbon atoms of tubulin only and in complex with 1,3-diynyl noscapinoids **20–22** during 100 ns of MD simulation. The relative fluctuation in the RMSD of the Cα atoms is very small after ~40 ns of the simulation, indicating stability of the system.

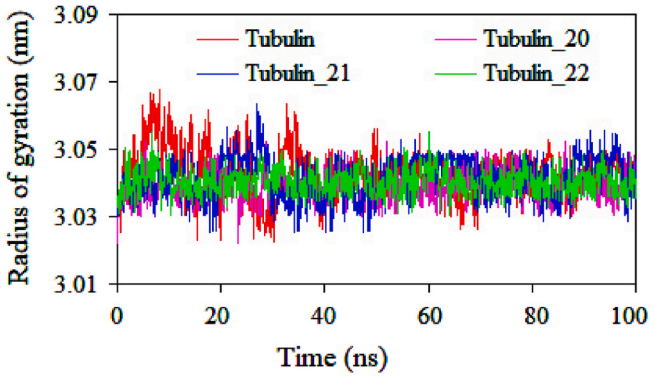

Fig. 7. Time evolution of radius of gyration of the tubulin and its complex with 1,3-diynyl derivatives of noscapine, **20–22** over a period of 100 ns of MD simulation. All the molecular systems were found to be stable after 40 ns of simulation.

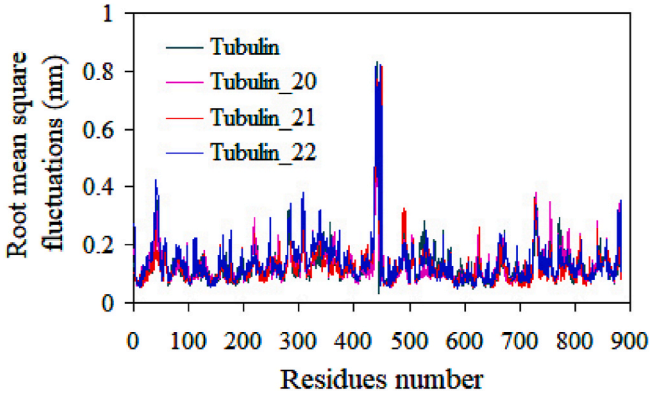

Fig. 8. Root mean square fluctuation (RMSF) of the residues of tubulin of the docked ligands in the bound form and in the unbound form of tubulin heterodimer. Different levels of flexibility of these residues were noticed in the free and bound form of tubulin with ligands. Only very few residues showed flexibilities >0.5 nm indicating that most of the residues were rigid both in free and bound form of tubulin.

ps to write 5000 frames for each molecular system. CPPTAJ implemented in Ambertools was used to analyze trajectories for root mean square deviation analyses. The top most 5 structures of the Tubulin-ligand complexes based on their lowest minimum total energy from the MD trajectory were used to generate an average structure to elucidate the binding mode and non-bonded interactions between the ligands and binding site amino acids.

2.7. Predictive binding affinity

Predicted binding energy ($\Delta G_{bind,pred}$) of 1,3-diynyl noscapinoids, **20–22** with tubulin was calculated using Molecular Mechanics Poisson-Boltzmann Surface Area (MM-PBSA) as the ensemble average of the binding free energy of a total of 1000 snapshots, extracted every 20 ps from the last 20 ns of the MD simulation trajectory as explained below:

$$\Delta G_{bind,pred} = \Delta G_{complex} - [\Delta G_{Rec} + \Delta G_{lig}]$$

$$G = E_{gas} + G_{sol} - TS$$

$$E_{gas} = E_{int} + E_{ele} + E_{vdw}$$

$$G_{sol} = G_{PB} + G_{sol\text{-}np}$$

$$G_{sol\text{-}np} = \gamma SAS$$

Where, G is Gibbs free energy, E_{gas} is the gas phase energy calculated as the sum of internal energy (E_{int}), E_{ele} is the electrostatic interaction energy and E_{vdw} is the van der Waals interaction energy. G_{sol} is the solvation free energy calculated as the sum of polar (G_{PB}) and nonpolar contributions ($G_{sol\text{-}np}$). Polar interaction contribution (G_{PB}) was calculated as the summation of electrostatic contribution (E_{ele}) and polar solvation contribution (G_{PB}). The nonpolar solvation contribution ($G_{sol\text{-}np}$) is approximated as linearly dependent on the solvent accessible surface area (SAS) and γ is the surface tension constant that was set to 0.0072 kcal/mol $Å^{-2}$.

2.8. Predicted ADME properties

The QikProp program (Schrodinger package) was used to predict the ADME properties of noscapine and its 1,3-diynyl derivatives **20–22.** All the compounds were imported into the project table and a set of 44 ADME properties were predicted. Some properties having zero values were manually deleted. The program also evaluates the acceptability of the compounds based on the Lipinski's rule of 5 (number of violations of Lipinski's rule of five) which is essential for rational drug design. Poor absorption or permeation are more likely when a ligand molecule violates Lipinski's rule of five i.e., has more than 5 hydrogen bond donors, the molecular weight is over 500, the log P is over 5 and the sum of N's and O's is over 10.

2.9. Chemical synthesis of 1,3-diynyl derivatives of noscapine, 20-22

The computationally screened 1,3-diynyl derivatives of noscapine, **20–22** were strategically synthesized from the lead molecule, noscapine as mentioned in Fig. 5. The detail procedure of chemical synthesis and the structural characterization of the molecules were mentioned in the supporting information (S2–S14). Structural characterization of all the intermediates and final products were done using NMR (^{1}H and ^{13}C), IR spectroscopy and mass (HRMS) spectrometry techniques. All the compounds are HPLC purified using C18 column (acetonitrile:water, 90:10) and is found to be >96.5%.

2.10. Cell culture and reagents

The natural lead compound, noscapine was obtained from Sigma. All the chemical reagents and media used for cell culture were obtained from Sigma. Human breast cancer cell line, MCF-7 and MDAMB-231

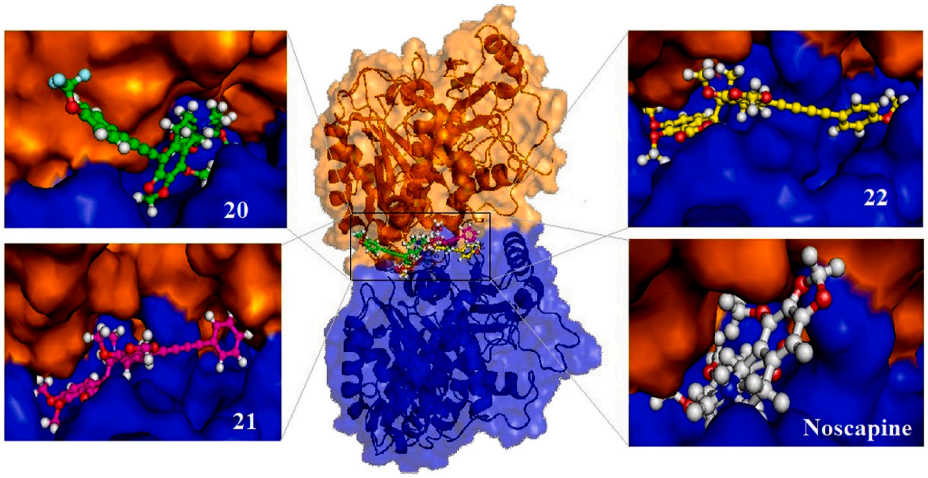

Fig. 9. The newly designed 1,3-diynyl noscapinoids, **20–22** and the lead molecule, noscapine are well accomodated inside the binding pocket at the interface of α- and β-tubulin. The binding site is represented as macromodel surface according to α- and β-tubulin (α-tubulin is represented in blue colour and β-tubulin is represented in brown colour). (For interpretation of the references to colour in this figure legend, the reader is referred to the Web version of this article.)

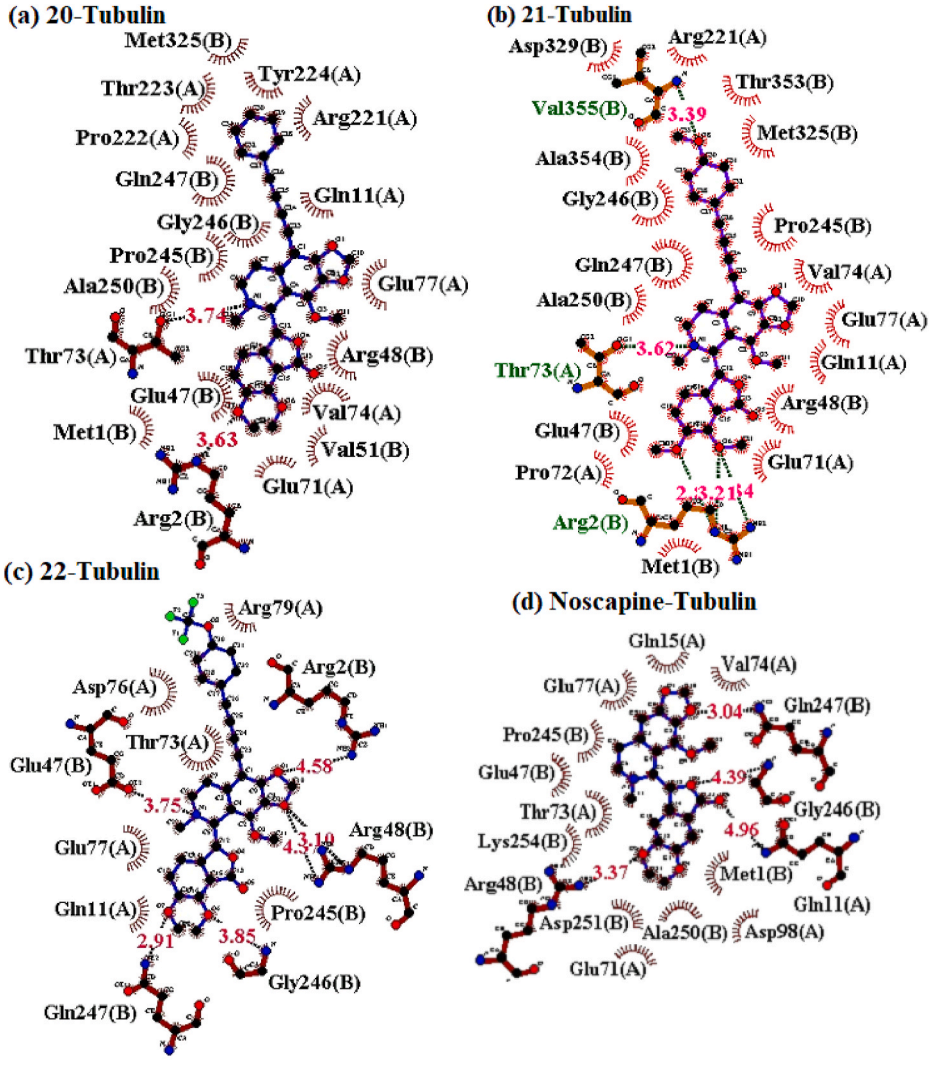

Fig. 10. Two dimensional representation of interaction observed between the binding site residues of tubulin with 1,3-diynyl noscapinoids **(a) 20, (b) 21, (c) 22** and **(d) Noscapine**. Dashed lines denote hydrogen bonds and numbers indicate hydrogen bond lengths in Å. Hydrophobic interactions are shown as arcs with radial spokes. The figure was made using LIGPLOT [18]. The residues within 5 Å distance from the docked ligands were only shown in the figures.

Table 1
Molecular docking results (Glide XP) as well as calculated energies using Liasion programme (Schrodinger package) of noscapine and its derivatives: van der Waals energy (U_{vdw}), Columbic energy (U_{coul}), reaction energy (U_{rxn}) and cavity energy (U_{cav}) as well as predicted binding free energy ($\Delta G_{bind,pred}$) based on LIE-SGB prediction model and experimental binding free energy ($\Delta G_{bind,expt}$). The newly designed 1,3-diynyl-noscapinoids, **20–22** revealed improved $\Delta G_{bind,pred}$ compared to the lead molecule, noscapine.

Ligand	Glide XP_{score} (kcal/mol)	$<U_{vdw}>$ (kcal/mol)	$<U_{coul}>$ (kcal/mol)	$<U_{rxn}>$ (kcal/mol)	$<U_{cav}>$ (kcal/mol)	$\Delta G_{bind,expt}$ (kcal/mol)	$\Delta G_{bind,pred}$ (kcal/mol)
Noscapine	−1.946	−44.84	−331.47	136.27	2.873	−5.246	−5.160
10	−2.558	−51.08	−212.38	118.43	3.763	−6.006	−6.161
11	−2.698	−43.17	−363.49	157.08	4.628	−5.827	−5.974
12	−2.633	−48.26	−357.08	169.38	3.188	−5.587	−5.803
13	−3.481	−48.09	−287.04	137.08	3.953	−6.360	−6.022
14	−4.793	−49.02	−79.05	119.42	4.084	−6.628	−6.478
15	−2.825	−35.18	−333.17	177.49	5.075	−5.551	−5.842
16	−2.385	−47.19	−278.47	114.07	4.176	−5.665	−5.872
17	−2.242	−34.92	−325.17	153.29	4.379	−5.783	−5.295
18	−3.668	−46.28	−470.38	154.17	3.865	−5.673	−5.572
19	−4.717	−43.57	−268.42	130.72	3.947	−5.518	−5.667
20	−2.522	−41.38	−317.5	161.5	5.864	–	−6.568
21	−4.101	−55.27	−304.6	127.4	5.946	–	−7.367
22	−5.028	−55.83	−258.3	125.3	6.847	–	−7.922

$<U_{vdw}>$, $<U_{coul}>$, $<U_{rxn}>$ and $<U_{cav}>$ energy terms represents the ensemble average energy terms calculated as the difference between bound and free state of the ligands and its environment.

Table 2
Binding free energy and its components (kcal/mol) for the receptor αβ tubulin dimer and noscapine derivatives binding to the active site of αβ tubulin dimer.

Energy components (kcal/mol)	Noscapine	20	21	22
ΔE_{vdw}	−56.22	−31.29	−41.81	−31.57
ΔE_{ele}	−202.5	−210.3	−177.6	−188.5
$\Delta G_{solv,PB}$	108.6	79.74	54.33	53.77
ΔG_{sol-np}	−6.19	−4.17	−4.82	−4.30
$\Delta G_{bind,\ PBSA}$	−156.3	−166.0	−169.7	−170.6

were obtained from the cell repository of the National Center for Cell Science Pune, Maharashtra, India. Stock solution (100 mM) of the newly synthesized noscapine derivatives, **20–22** was prepared with dimethyl sulfoxide (DMSO) and stored at 4 °C until use. The cells were allowed to grow at a temperature of 37 °C in a 5% CO_2 and 95% humidity in Dulbecco's modified Eagle medium (DMEM, Pan Biotech), supplemented with 10% fetal bovine serum (FBS) and antibiotics. Cells with a 70–80% confluence were sub cultured for bioassays using trypsin-EDTA (0.25%).

2.11. In vitro cell proliferation assay using MCF-7 and MDAMB-231 cell lines

The cell proliferation assay was performed in 96-well plates as described previously using two human breast cancer cell lines, MCF-7 and MDAMB-231 [38]. In brief, cells were grown in culture medium (MEM, DMEM) supplemented with 10% fetal bovine serum, 1% penicillin/streptomycin, 2 mM L-glutamine at 37 °C in a humidified atmosphere with 5% CO_2. Suspension cells were plated into 96-well plates at a density of 5×10^3 cells per well and were treated with gradient concentrations (5 μM–100 μM) of noscapine and its derivatives **20–22** for 72 h. The cells were then fixed with 50% trichloroacetic acid and stained

Table 4
IC_{50} values of novel 1,3-diynyl-noscapinoids, **20–22** using two human breast adenocarcinoma cell lines, MCF-7 and MDAMB-231. All the novel derivatives were found to have improved antiproliferative activity compared to noscapine.

	IC_{50} (μM)			
	Noscapine	20	21	22
MCF-7	45.0 ± 4.3	16.7 ± 2.2	11.8 ± 1.5	7.9 ± 0.6
MDAMB-231	58.3 ± 5.2	29.0 ± 2.7	19.2 ± 1.8	10.2 ± 1.3

Table 3
A list of properties calculated for Noscapine and its 1,3-diynyl derivatives by Qikprop simulation and used for the ADME screening of the drug molecules. It was found that noscapine and its 1,3-diynyl derivatives **20–22** satisfied all the properties essential for ADME screening.

Sl No.	ADME Screening	Noscapine	20	21	22	Recommended values
1	MW	413.4	621.6	537.6	567.6	130–725
2	SASA	638.0	917.8	853.9	451.9	548.0
3	Accpt HB	8.75	8.75	8.75	9.5	2.0–20.0
4	QPpolrz	40.0	61.0	57.1	58.9	13.0–70.0
5	QPlogPoct	17.62	25.27	23.33	24.21	8.0–35
6	QPlogPw	10.22	11.61	12.02	12.16	4.0–45.0
7	QPlogPo/w	1.95	6.05	4.88	4.96	−2.0–6.5
8	QPlogHERG	−5.214	−7.643	−7.729	−7.455	Below −5.0
9	QPPCaco	799.2	738.2	900.6	960.2	<25 poor >500 great
10	QPlogBB	0.299	0.243	0.137	0.107	−3.0–1.2
11	QPPMDCK	429.5	1792.5	488.8	523.8	<25 poor >500 great
12	QPlogKp	−3.907	−3.008	−2.7	−2.775	−8.0–−1.0
13	QPlogKhsa	−0.429	0.975	0.639	0.616	−1.5–1.5
14	QP%	90.32	87.79	95.46	96.39	>80% high <25% poor
15	Rule of Five (No. of violations)	0	2	1	1	Maximum is 4

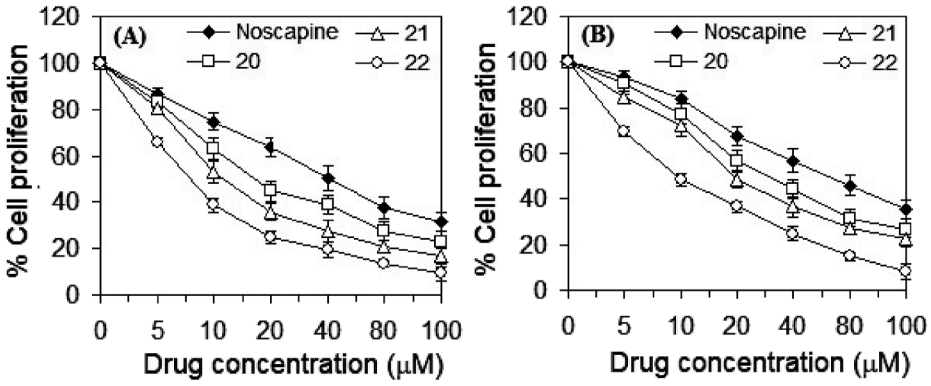

Fig. 11. The 1,3-diynyl-noscapinoids, **20–22** are more active compared to noscapine in inhibiting the proliferation of human breast cancer cells. Both (A) MCF-7 and (B) MDAMB-231 cells were treated with noscapine and its 1,3-diynyl-noscapinoids, **20–22**, for 72 h and reduction in cellular proliferation was measured. Each value represents the average of 3 independent experiments. 1,3-diynyl-noscapinoids, 20–22 inhibits proliferation of primary breast cancer cells.

Table 5
IC_{50} values of novel 1,3-diynyl-noscapinoids, **20–22** using primary breast cancer cells isolated from breast tumor tissue of different patients. All the novel derivatives were found to have improved antiproliferative activity compared to noscapine.

IC_{50} (μM)				
Patients No.	Noscapine	20	21	22
P-1	46.1 ± 4.6	20.3 ± 1.7	11.7 ± 1.3	7.3 ± 0.6
P-2	45.6 ± 4.1	21.1 ± 1.5	12.0 ± 1.2	8.1 ± 0.9
P-3	49.6 ± 4.8	22.8 ± 2.4	11.4 ± 1.5	7.2 ± 0.5
P-4	44.2 ± 4.2	16.7 ± 1.9	8.6 ± 0.7	5.3 ± 0.4
P-5	41.6 ± 4.7	17.5 ± 2.3	9.4 ± 0.6	5.4 ± 0.6
P-6	47.9 ± 4.1	17.2 ± 2.1	10.5 ± 1.2	6.8 ± 0.4
P-7	46.8 ± 3.9	17.9 ± 1.8	10.1 ± 0.9	6.5 ± 0.7
P-8	44.2 ± 3.7	16.5 ± 1.7	8.6 ± 0.8	5.3 ± 0.5

with 0.4% sulforhodamine B dissolved in 1% acetic acid. The cells were then washed with 1% acetic acid to remove unbound dye. The protein bound dye was extracted with 10 mM Tris base to determine the optical density at 564 nm wavelength using a microplate spectrophotometer. The IC_{50} values that stand for drug concentration required to achieve 50% cell lysis was determined using online tool Quest GraphTM IC_{50} Calculator (AAT Bioquest, Inc., Sunnyvale, CA, USA, https://www.aatbio.com/tools/ic50-calculator).

2.12. Primary breast cancer cells (PBCs) culture and in vitro cell proliferation assay

Primary breast cancer cells were obtained from the patients (8 nos.) of different stages of breast cancer before drug treatment in aseptic condition. The tumour tissues were treated with 0.25% trypsin and filtered with 70 μm filter followed by centrifugation at 2000 rpm for 3 min with serum free medium. The filtered cells were collected and plated in T25 flask and incubated with complete DMEM medium, supplemented with 10% FBS and 1% pentrip (mixture of penicillin and streptomycin) at 37 °C under 5% CO_2. Fresh media was replaced every 3–4 days, and subsequent passaging was performed under the same conditions as mentioned above. The cultured were maintained for homogeneous cell type at sub-confluence between 3 - 8 passages. Cells were allowed to reach 80–90% confluence prior to experimental treatments. After the confluence reached, the primary cells were plated at 2000 cells/well in 96 wells plate with standard growth media, DMEM (low glucose). The cells were maintained at 37 °C in a humidified atmosphere with 5% CO_2 and were treated with gradient concentrations (5 μM–100 μM) of noscapine and its derivatives, **20–22** for 72 h. Measurement of cell proliferation was performed with a colorimeter by sulforhodamine B (SRB) assay, using the CellTiter96 AQueous One Solution Reagent (Sigma). Cells will be exposed to SRB for 30 min followed by washing of unbound dye and adding 1 mM tris and absorbance (optical density) was measured using a microplate reader (Molecular Devices, Sunnyvale, CA) at a wavelength of 564 nm. The percentage of cell survival as a function of drug concentration were then plotted to determine the IC_{50} value.

2.13. Flow cytometry analysis of cell cycle progression

MDAMB-231 cells were maintained in Dulbecco's Modification of Eagle's Medium (DMEM) with 4.5 g/l glucose and L-glutamine supplemented with 10% fetal bovine serum and 1% penicillin/streptomycin. Cells were grown at 37 °C in a 5% CO_2 atmosphere. Cells were treated with noscapine and its derivatives, **20–22** dissolve in 1% phosphate buffer saline (PBS). Cells were sampled after 72 h of treatment, followed by analysis using flow cytometry. Briefly, 2×10^6 cells was centrifuged, washed twice with ice-cold phosphate-buffered saline (PBS), and fixed in 70% ethanol. Tubes containing the cell pellets were stored at −20 °C for 24 h. After this, the cells were centrifuged at 1000×*g* for 10 min and the supernatant was discarded. The pellet was resuspended in 30 μl of phosphate/citrate buffer (0.2 M Na_2HPO_4/0.1 M citric acid, pH 7.5) at room temperature for 30 min. Cells were then washed with 5 ml of PBS and incubated with 0.5 ml of propidium iodide (20 μg/ml in 0.6% Triton-X in PBS) and 0.5 ml of RNase A (20 μg/ml in PBS) for 45 min in dark. Samples were analysed on a flow cytometer (BD FACS Aria-III) and the progress in the cell cycle was determined.

2.14. Flow cytometry analysis for apoptosis assay

During apoptosis, choline phospholipids such as phosphatidylcholine and sphingomyelin (PS) are exposed on the external leaflet, while aminophospholipids (phosphatidylserine, phosphatidylethanolamine) are exclusively located on the cytoplasmic surface of the lipid bilayer. The detection of PS by fluorochrome-tagged 36 KDa anticoagulant protein Annexin V allows for a precise estimation of apoptotic incidence. This probe reversibly binds to phosphatidylserine residues only in the presence of mM concentration of divalent calcium ions.

Apoptosis in cancer cells was detected by Annexin-V-FITC detection kit (Sigma –Aldrich, USA) based on instruction provided by manufacture. In brief, 3×10^4 MDAMB-231 cells per well were seeded on 12 well culture plate and incubated for 24 h with complete medium. The cells were treated with IC_{50} concentration of noscapine and its derivatives, **20–22** and were harvested after 48 h. Cells were typsinized and stained with surface marker antibodies (biotin-conjugated Annexin V, FITC-conjugated streptavidin) and propiumdium iodide (PI). Cells were allowed to suspend in 1X binding buffer and incubated with Annexin-V-FITC conjugate for 20 min in dark condition at room temperature. Flow

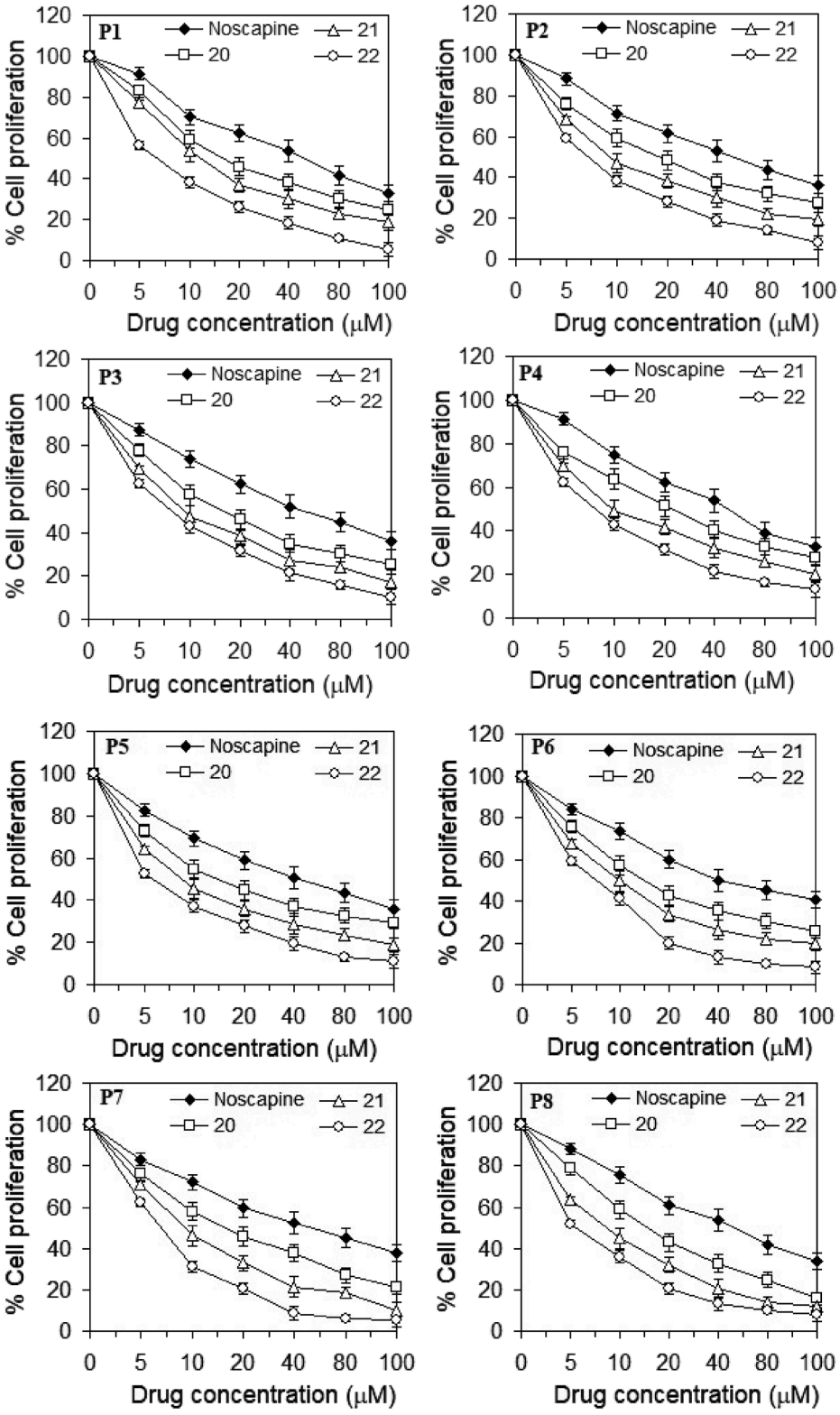

Fig. 12. The 1,3-diynyl-noscapinoids, **20–22** are more active compared to noscapine in inhibiting the proliferation of a panel of human primary breast tumor cells obtained from breast cancer patients (P-1 to P-4). All the cells were treated with 1,3-diynyl-noscapinoids, **20–22** for 72 h and measured their reduction in cellular proliferation. Each value represents the average of 3 independent experiments.

cytometer data with 488 nm excitation for PI and emission at 530 nm were collected. Viable cells (Annexin V^-/PI^-), early apoptotic cells (Annexin V^+/PI^-), late apoptotic/necrotic cells (Annexin V^+/PI^+) and late necrotic cells (Annexin V^-/PI^+) were identified and determined their percentage.

2.15. DAPI staining

Cell morphology was evaluated by fluorescence microscopy following DAPI staining. MDAMB-231 cells were grown on poly-L-lysine coated coverslips in 6-well plates and were treated with noscapine and

Table 6
Percentage of early apoptotic (Q1), late apoptotic (Q2), viable (Q3) and necrotic (Q4) cell measured by flow cytometry.

Viability/Apoptotic	Control	20	21	22
Q1	5%	30%	20%	23%
Q2	2%	10%	30%	36%
Q3	91%	50%	42%	35%
Q4	2%	3%	5%	15%

its derivatives, **20–22** at 25 μM for 72 h. After incubation, coverslips were fixed in cold methanol and washed with PBS, stained with DAPI, and mounted on slides. Images were captured using an inverted fluorescence microscope (Nikon) with imagining system. Apoptotic cells were identified by features characteristic of apoptosis (e.g. nuclear condensation, formation of membrane blebs and apoptotic bodies).

3. Results and discussion

The effectiveness in terms of cell killing of the lead compound, noscapine was improved many fold by synthesizing many potent derivatives. These derivatives were proven to have increased tubulin binding affinity as indicated by their lower dissociation constants (K_d) from 152 μM for noscapine to 86 μM for nitro noscapine, 80 μM for F-noscapine, 54 μM for Br-noscapine, 40 μM for Cl-noscapine, 22 μM for I-noscapine and 14 μM for amino-noscapine [14,22,43,44]. Furthermore, we have made some effective derivatives of noscapine by functionalization of 'N' in isoquinoline unit of natural α-noscapine [45] as well as a series of biaryl pharmacophore inserted noscapine derivatives as potent anticancer agents [19]. Availability of structure activity data of these

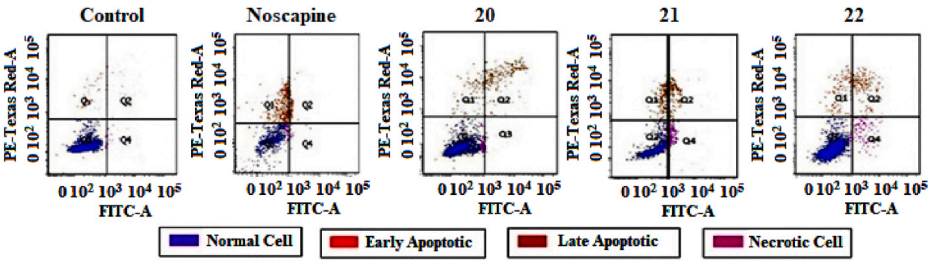

Fig. 13. Flow cytometry analysis of phosphatidylserine (PS) exposure in MDAMB- 231 cells treated with noscapine and 1,3-diynyl noscapinoids (**20–22**) with 25 μM for 72 h and compared with non-treated control cells. Alexa Fluor 488 conjugate of Annexin-V was used in combination with the non-vital dye propidium iodide (PI) to distinguish among three sub-populations: PI-negative and Alexa Fluor 488-negative viable cells with intact membrane and preserved amino-phospholipid asymmetry (PI-, Alexa Fluor 488-), PI-negative and Alexa Fluor 488-positive early apoptotic cells with intact cellular membrane exposing phosphatidylserine (PI-, Alexa Fluor 488+), and PI-positive and Alexa Fluor 488-positive late apoptotic cells with compromised asymmetry and membrane permeability (PI+, Alexa Fluor 488+). The representative results of three independent experiments.

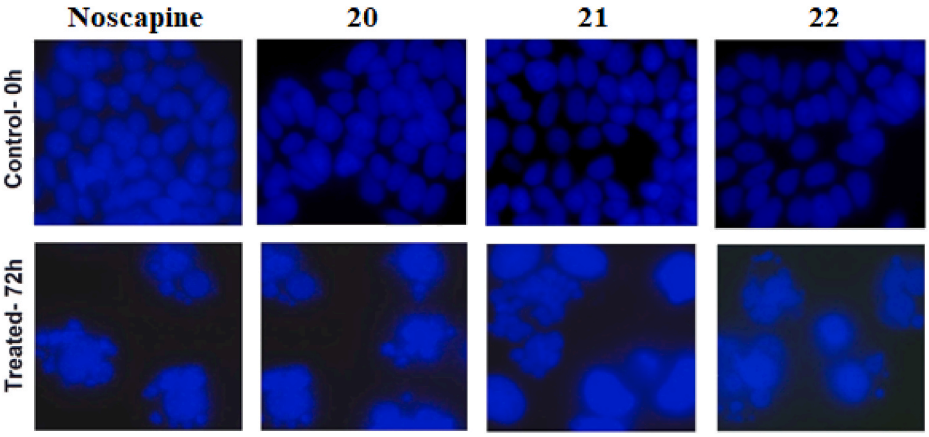

Fig. 14. Morphologic criteria for apoptotic cell death include chromatin condensation with aggregation in nuclear envelope and plasma membrane blebbing followed by separation into small apoptotic bodies. Panels showed the morphological evaluation of nuclei stained with DAPI from control cells (upper panels) and cells treated with 25 μM concentration of noscapine and newly designed 1,3-diynyl noscapinoids (**20–22**) (lower panels) for 72 h using fluorescence microscopy. Several typical features of apoptotic cells such as condensed chromosomes, numerous fragmented micronuclei, and apoptotic bodies were evident upon 72 h of drug treatment.

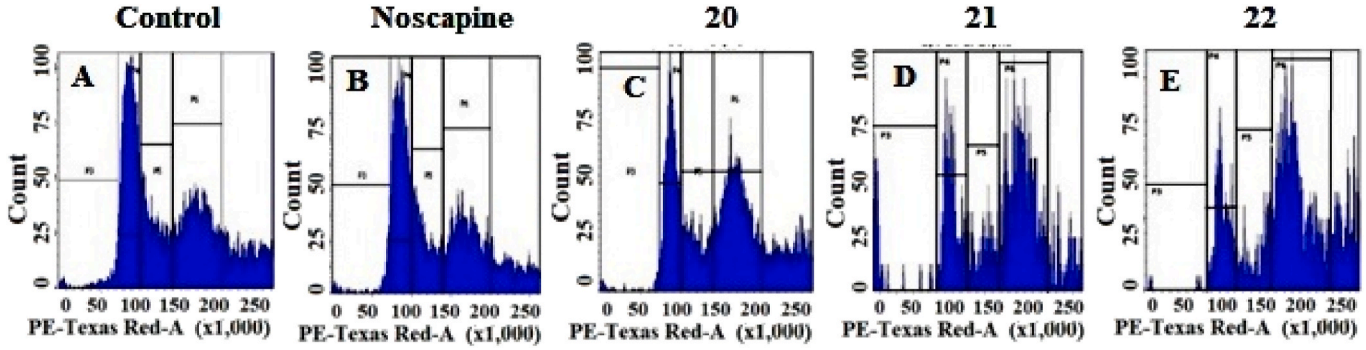

Fig. 15. Noscapine and the newly developed 1,3-diynyl noscapinoids (**20–22**) inhibit cell cycle progression at mitosis followed by the appearance of characteristic hypodiploid (sub-G1) DNA peak, which was indicative of apoptosis. Panels A-E depict analyses of cell cycle distribution as determined by flow cytometry in MDAMB-231 cells treated with 25 μM noscapine and its derivatives (**20–22**) at 72 h of treatment.

Table 7
Effect of noscapine and its 1,3-diynyl derivatives (**20–22**) on cell cycle progression of MDAMB-231 breast cancer cells treated with 25 μM concentration exposed for 72 h before being stained with propidium iodide for cell cycle analysis.

	MDAMB-231 cells treated with 25 μM for 72 h			
	Sub-G_1	G_0/G_1	S	G_2/M
Untreated	0.5	15.0	22.5	9.6
Noscapine	5.3	13.5	13.4	21.4
20	9.5	16.2	9.5	27.2
21	14.3	18.7	8.6	30.7
22	19.7	22.3	11.2	34.8

derivatives of noscapine led us to develop a reasonable predictive model for predicting the binding affinity of newly designed derivatives and screening. In continuation of our efforts to develop new derivatives of noscapine, we are reporting in this study a panel of 1,3-diynyl-noscapinoids, **20–22** as potent anticancer agents.

3.1. Molecular modeling evaluation of designed 1,3-diynyl noscapinoids

The lead molecule, noscapine, its previously reported derivatives (Fig. 3) and newly designed 1,3-diynyl-noscapinoids (Fig. 2) were docked onto tubulin on its reported binding site of noscapinoids [23,25] using Glide XP (extra precision) and evaluated using a Glide XP_{score} function [39,40]. The newly designed 1,3-diynyl derivatives of noscapine docked well at the interface between α- and β-tubulin and showed relatively better docking scores compared to noscapine and its previously reported derivatives. Further, the binding affinity ($\Delta G_{bind,pred}$) of 1,3-diynyl-noscapinoids with tubulin was predicted based on computationally developed linear interaction energy model (LIE), utilizing the experimental activity of training set molecules (Table 1). Since the molecular docking predicts accurate binding pose for the ligands onto the receptor, we have used the docking complexes of noscapinoids with tubulin and performed hybrid Monte Carlo simulation with generalized Born (SGB) continum solvation model to develop a robust predictive model. The various interaction energy terms used in the model were included in Table 1 and were used to develop the LIE model. The values obtained for the four fitting parameters, α, β, γ and δ are 0.0747, −0.0022, −0.0090 and −0.4702, respectively. The largest contribution for the binding free energy comes from the Columbic interactions. The predicted $\Delta G_{bind,pred}$ of the training set molecules based on LIE-SGB model is very close to the experimental $\Delta G_{bind,expt}$ (root mean square error was 0.302 kcal/mol). The quality of the fit can also be judged by the value of the squared correlation coefficient (R^2) and analysis of variance (F-value).

$$\Delta G_{bind,pred} = 0.0747\langle U_{vdw}\rangle - 0.0023\langle U_{coul}\rangle - 0.0090\langle U_{rxn}\rangle - 0.4702\langle U_{cav}\rangle$$

$$(n = 11,\ R^2 = 0.999,\ s = 0.302,\ F = 1019.5,\ P \leq 0.001)$$

Because of high predictability, the LIE model was used to predict the $\Delta G_{bind,pred}$ of the newly designed 1,3-diynyl-noscapinoids. Finally a panel of three 1,3-diynyl-noscapinoids, **20–22** that revealed improved predicted binding energy of −6.568 kcal/mol for **20**, -7.367 kcal/mol for **21** and -7.922 kcal/mol for **22**, respectively in comparison to the lead molecule (−5.246 kcal/mol) were screened out for chemical synthesis and experimental evaluation.

3.2. MD simulations and predicted binding free energy using MM-PBSA

The docked complexes of 1,3-diynyl-noscapinoids, **20–22** with tubulin were used to performed MD simulations of 100 ns to observed the stability of the molecular system. The ligands were fund to bind with the tubulin for the entire period of simulation. The convergence of the MD trajectories was monitored by plotting root mean square deviation (RMSD) and radius of gyration (Rg) of the backbone C_α atoms with respect to time. The RMSD and the Rg values were very small after ~40 ns suggesting the stability of the system (Fig. 6 and Fig. 7). It was also observed that the root mean square fluctuations (RMSF) of most of the residues of tubulin in the free and bound form with ligands ranges from 0 to 0.4 nm, indicating that the residues were more rigid. However, only very few residues showed fluctuation >0.5 nm, indicating that these residues seem to be more flexible (Fig. 8). All the three 1,3-diynyl-noscapinoids, **20–22** were found to accommodate well inside the binding cavity (Fig. 9) at the interface between α- and β-tubulin. However, their binding modes inside the binding cavity are distinct compared to noscapine as shown in the ligplot (Fig. 10 a-d). The differences in binding modes of these noscapinoids are due to various substitutions of functional groups in the scaffold structure. As showed in the figure the most potent 1,3-diynyl noscapinoid **22** in terms of docking score and $\Delta G_{bind,pred}$ interacts more intensely with the residues of tubulin compared to other two derivatives. Its binding involved 6 hydrogen bonds (dashed lines): the O7 of **22** H-bonded with NE2 of Gln B247 (bond length 2.91 Å), O6 of **22** H-bonded with N of Gly B246 (bond length 3.85 Å), O2 of **22** H-bonded with NH2 of Arg B48 (bond length 4.37 Å) and NE of Arg B48 (bond length 3.1 Å), N1 of **22** H-bonded with OE2 of Glu B47 (bond length 3.75 Å) and O1 of **22** H-bonded with NH2 of Arg B2 (Fig. 10c). In contrast the 1,3-diynyl noscapinoids **20** and **21** revealed only 2 and 5 hydrogen bonds, respectively with the binding site residues (Fig. 10a and b). Besides, hydrogen bonding, good number of hydrophobic interactions were involved in the binding of 1,3-diynyl noscapinoids **20–22** with binding site residues (Supplementary Tables S15–S18).

The predictive binding free energy ($\Delta G_{bind,pred}$) of noscapine and its 1,3-diynyl noscapinoids, **20–22** according to MM-PBSA is collated in Table 2. It is revealed that the newly designed 1,3-diynyl noscapinoids, **20–22** have high $\Delta G_{bind,pred}$ compared to noscapine. Both the intermolecular van der Waals (ΔE_{vdw}) and the electrostatic (ΔE_{ele}) interactions were found to be significant contributors to the binding energy. Also the non-polar solvation terms ($\Delta G_{sol\text{-}np}$), which define the burial of solvent-accessible surface-area upon binding was somewhat favorable to the binding of ligands. In contrast, the polar solvation terms ($\Delta G_{sol\text{-}PB}$) was not favorable to the binding of ligands. This might be due to the large desolvation penalty of charged and polar groups that are not sufficiently compensated by complex formation.

3.3. Predicted ADME properties of noscapine and its 1,3-diynyl derivatives 20-22

In order to validate the lead optimization, we have predicted the absorption, distribution, metabolism, and excretion (ADME) properties of noscapine and its 1,3-diynyl derivatives **20–22** using QikProp (Schrodinger software package). A number of ADME properties were predicted viz. molecular weight (MW), total solvent accessible surface area (SASA), octanol/water partition coefficient (QPlogPo/w), octanol/gas partition coefficient (QPlogPoct), water/gas partition coefficient (QPlogPw), polarizability in cubic angstroms (QPpolrz), % human oral absorption in intestine (QP%), brain/blood partition coefficient (QPlogBB), IC_{50} value for blockage of HERG K+ channel (QPlogHERG), skin permeability (QPlogKp), prediction of binding to human serum albumin (QPlogKhsa), apparent Caco-2 cell permeability in nm/sec (QPPCaco) and apparent MDCK cell permeability in nm/sec (QPPMDCK). Caco-2 cells are a model for the gut-blood barrier whereas MDCK cells are considered to be a good mimic for the blood-brain barrier. Also we evaluated the acceptability of noscapine and its 1,3-diynyl derivatives **20–22** based on the Lipinski's rule of 5 (number of violations of Lipinski's rule of five) which is essential for rational drug design. It was interesting to found that noscapine and its 1,3-diynyl derivatives **20–22** revealed significant values for the properties analysed and qualified all the drug like characteristic based on Lipinski's

rule of 5 (Table 3).

3.4. Newly designed noscapinoids inhibits proliferation of cancer cells, MCF-7 and MDAMB-231

Based on our *in silico* results, we focused at the cellular level to determine if the 1,3-diynyl-noscapinoids, **20–22,** affected cancer cell proliferation. All the 3 compounds, **20–22** including the parent compound, noscapine were analysed for their anti-proliferative activity in two human breast adenocarcinoma cells, MCF-7 (estrogen- and progesterone-receptor positive) and MDAMB-231 (estrogen- and progesterone-receptor negative). The IC_{50} values for the test compounds for both the cell lines are collated in Table 4. All the 1,3-diynyl-noscapinoids, **20–22** exhibited potent cytotoxic activity in comparison to noscapine using both the cell lines (Fig. 11). The IC_{50} value amounted to 45.0 μM, 16.7 μM, 11.8 μM and 7.9 μM with noscapine, **20, 21** and **22**, respectively for MCF-7 cells, which reflects a modest anti-proliferative activity. Parenthetically, a similar modest IC_{50} value of 58.3 μM, 29.0 μM, 19.2 μM and 10.2 μM was measured for noscapine, **20, 21** and **22**, respectively for MDAMB-231 cells. The significant differences in IC_{50} values obtained using MCF-7 and MDAMB-231 to these analogs were cell-type dependent. Although a significant correlation on the sensitivity of cancer cells to these analogs cannot yet be established at this stage, it is evident that tubulin represents a potential target for these compounds.

We next want to evaluate whether the newly developed 1,3-diynyl-noscapinoids, **20–22** could also inhibit the proliferation of primary cancer cells directly isolated from patients. We have obtained the surgically removed breast tumor samples from 08 different patients with different stages of breast cancer and processed the samples to isolate the primary cancer cells. All these primary breast cancer cells were treated with increasing concentrations of the noscapinoids to determine their IC_{50} value. The IC_{50} values for the test compounds are collated in Table 5. The IC_{50} value ranges from 44.2 to 49.6 μM for noscapine, 16.7–22.8 μM for **20**, 8.6–12.0 μM for **21** and 5.3–8.1 μM for **22** using a panel of primary breast cancer cells (Table 5). All the 1,3-diynyl-noscapinoids developed exhibited potent cytotoxic activity in comparison to noscapine using all the primary breast cancer cells (Fig. 12).

Fig. 12(continued). The 1,3-diynyl-noscapinoids, **20–22** are more active compared to noscapine in inhibiting the proliferation of a panel of human primary breast tumor cells obtained from breast cancer patients (P-5 to P-8). All the cells were treated with 1,3-diynyl-noscapinoids, **20–22** for 72 h and measured their reduction in cellular proliferation. Each value represents the average of 3 independent experiments.

3.5. 1,3-Diynyl-noscapinoids, 20–22 induced apoptosis to cancer cells

The induction of apoptotic cell death to breast cancer cell by the newly developed 1,3-diynyl noscapinoids, **20–22** was determined. Apoptotic process is characterized by the alterations in lipid composition of cell membrane *i.e.* phosphatidylserine, which is normally on the inner leaflet of cell membrane translocates to outer leaflet, which can be measured using Annexin V by fluorescent binding. In contrast, the cell impairment DNA-binding fluorescent dye *i.e.* propidium iodide can only enter the cells at the stage of late apoptosis when membrane permeability is compromised. Apoptotic cells can be quantified by FACS analysis. The percentage of early and late apoptotic cells using MDAMB-231 cell lines for treatment with 25 μM noscapine and its diyne noscapinoids (**20–22**) for 72 h is collated in Table 6. Corresponding figures of flow cytometry analysis treated with noscapine and its diyne derivatives (**20–22**) were represented in Fig. 13. After 72 h, the control untreated cell culture represented only few early apoptotic (2.5%) and late apoptotic cells (1.0%), which were considered as the background cell death due to regular trauma during cell culture (Table 6). In contrast, the percentage of early apoptotic cells of 30%, 20%, 23%, 27%; late apoptotic cells of 10%, 30%, 36%, 39% and necrotic cells of 3%, 5%, 15% and 12% treated with noscapine and its 1,3-diynyl noscapinoids (**20–22**), respectively were found to be relatively higher compared to the controlled untreated cells (Table 6).

Besides, the morphological examination using DAPI staining revealed apoptotic cell death of MDAMB-231 breast cancer cells characterized by chromatin condensation along with the appearance of numerous fragmented nuclei (Fig. 14).

3.6. 1,3-Diyne noscapinoids (20–22) alter cell cycle and mitotic arrest

Effect of noscapine and 1,3-diyne noscapinoids (**20–22**) at a concentration of 25 μM on cell cycle profile of MDAMB-231 based on FACS analysis was examined to ascertain the mechanism of cell death (Fig. 15). The fluorescently labelled DNA accumulation is considered as good indicator of cell cycle progression and cell death. The unreplicated complement of 2 N DNA cells represent the G1 phase, while duplicated 4 N DNA cells represent G2 and M phases. The cells during DNA duplication between 2 N and 4 N peaks represent S phase when DNA is being synthesized. Less than 2 N DNA appears in populations of dying cells that degrade their DNA to different extent. The treatment of MDAMB-231 cells for 72 h with the test compounds treated with 25 μM led to significant perturbations of cell cycle profile. FACS analysis revealed high accumulation of cells during the G2M phase at 72 h of treatment with noscapine and the newly developed derivatives of noscapinee (**20–22**) compared to the untreated cells (Table 7). In contrast to G2/M block, the characteristic hypodiploid DNA content peak (sub-G1) was observed to rise at 72 h of treatment. The progressive generation of cells having hypodiploid DNA content reflects the existence of fragmented DNA indicating dying cells.

4. Conclusion

In conclusion, we have strategically design potent derivatives of natural lead molecule, noscapine in quest of increasing its anticancer activity. We have also provided simplest methods for the direct and regioselective modification of noscapine scaffold to produce the 1,3-diyne derivatives in high yields. All the three diyne derivatives developed have showed increase anticancer activity based on our extensive molecular modeling and cellular study using two human breast cancer cell lines, MCF-7 and MDAMB-231. Therefore, these novel compounds may prove efficacious not only in the treatment of breast carcinoma, but also for other type of cancers. Our results compel us to continue to examine the effects of these novel compounds on in vivo animal experiment with the final goal of taking it to the human clinical study.

Declaration of competing interest

The authors declare that they have no known competing financial interests or personal relationships that could have appeared to influence the work reported in this paper.

Acknowledgement

We would like to acknowledge the financial support provided by the OHEPEE, Govt. of Odisha, India through World Bank under Center of Excellence in Natural Products and Therapeutics, Sambalpur University.

Appendix A. Supplementary data

Supplementary data to this article can be found online at https://doi.org/10.1016/j.jmgm.2021.107933.

References

[1] E.K. Rowinsky, The development and clinical utility of the taxane class of antimicrotubule chemotherapy agents, Annu. Rev. Med. 48 (1997) 353–374.

[2] Pace, L. Bove, C. Nistico, M. Ranuzzi, P. Innocenti, A. Pietrangeli, E. Terzoli, B. Jandolo, Vinorelbine neurotoxicity: clinical and neurophysiological findings in 23 patients, J. Neurol. Neurosurg. Psychiatr. 61 (1996) 409–411.
[3] J. Crown, M. O'Leary, The taxanes: an update, Lancet 355 (2000) 1176–1178.
[4] K. Meller Theiss, Taxol impairs anterograde axonal transport of microinjected horseradish peroxidase in dorsal root ganglia neurons in vitro, Cell Tissue Res. 299 (2000) 213–224.
[5] K.S. Topp, K.D. Tanner, J.D. Levine, Damage to the cytoskeleton of large diameter sensory neurons and myelinated axons in vincristine-induced painful peripheral neuropathy in the rat, J. Comp. Neurol. 424 (2000) 563–576.
[6] K. Ye, Y. Ke, N. Keshava, J. Shanks, J.A. Kapp, R.R. Tekmal, J. Petros, H.C. Joshi, Opium alkaloid noscapine is an antitumor agent that arrests metaphase and induces apoptosis in dividing cells, Proc. Natl. Acad. Sci. U.S.A. 95 (1998) 1601–1606.
[7] J. Zhou, M. Liu, R. Aneja, R. Chandra, H. Lage, H.C. Joshi, Reversal of P-glycoprotein-mediated multidrug resistance in cancer cells by the c-jun NH2-terrminal kinase, Can. Res. 66 (2006) 445–452.
[8] Dahlstrom, T. Mellstrand, C.G. Lofdahl, M. Johansson, Pharmacokinetic properties of noscapine, Eur. J. Clin. Pharmacol. 22 (1982) 535–539.
[9] M.O. Karlsson, B. Dahlstrom, S.A. Eckernas, M. Johansson, A.T. Alm, Pharmacokinetics of oral noscapine, Eur. J. Clin. Pharmacol. 39 (1990) 275–279.
[10] L.N. Jensen, L.L. Christrup, L. Jacobsen, J. Bonde, H. Bundgaard, Relative bioavailability in man of noscapine administered in lozenges and mixture, Acta Pharm. Nord. 4 (1992) 309–312.
[11] J. Zhou, P. Giannakakou, Targeting microtubules for cancer chemotherapy, Curr. Med. Chem. Anti Canc. Agents 5 (2005) 65–71.
[12] J.W. Landen, R. Lang, S.J. McMahon, N.M. Rusan, A.M. Yvon, A.W. Adams, M. D. Sorcinelli, R. Campbell, P. Bonaccorsi, J.C. Ansel, D.R. Archer, P. Wadsworth, C. A. Armstrong, H.C. Joshi, Noscapine alters microtubule dynamics in living cells and inhibits the progression of melanoma, Can. Res. 62 (2002) 4109–4114.
[13] J. Zhou, D. Panda, J.W. Landen, L. Wilson, H.C. Joshi, Minor alteration of microtubule dynamics causes loss of tension across kinetochore pairs and activates the spindle checkpoint, J. Biol. Chem. 277 (2002) 17200–17208.
[14] R. Aneja, S.N. Vangapandu, M. Lopus, R. Chandra, D. Panda, H.C. Joshi, Development of a novel nitro-derivative of noscapine for the potential treatment of drug-resistant ovarian cancer and Tcell lymphoma, Mol. Pharm. 69 (2006) 1801–1809.
[15] R. Aneja, N. Dhiman, J. Idnani, A. Awasthi, S.K. Arora, R. Chandra, H.C. Joshi, Preclinical pharmacokinetics and bioavailability of noscapine, a tubulin-binding anticancer agent, Canc. Chemother. Pharmacol. 60 (2007) 831–839.
[16] Y. Ke, K. Ye, H.E. Grossniklaus, D.R. Archer, H.C. Joshi, J.A. Kapp, Noscapine inhibits tumor growth with little toxicity to normal tissues or inhibition of immune responses, Canc. Immunol. Immunother. 49 (2000) 217–225.
[17] R. Aneja, T. Miyagi, P. Karna, T. Ezell, D. Shukla, M.V. Gupta, H.C. Joshi, A novel microtubule-modulating agent induces mitochondrially driven caspase-dependent apoptosis via mitotic checkpoint activation in human prostate cancer cells, Eur. J. Canc. 46 (2010) 1668–1678.
[18] T. Mahaddalkar, P.K. Naik, S. Choudhary, N. Manchukonda, S. Kantevari, M. Lopus, Structural investigations into the binding mode of a novel noscapine analogue, 9-(4-vinylphenyl) noscapine, with tubulin by biochemical analyses and molecular dynamic simulations, J. Biomol. Struct. Dynam. 35 (2017) 2475–2482.
[19] S. Santoshi, N.K. Manchukonda, C. Suri, M. Sharma, B. Sridhar, S. Joseph, M. Lopus, S. Kantevari, I. Baitharu, P.K. Naik, Rational design of biaryl pharmacophore inserted noscapine derivatives as potent tubulin binding anticancer agents, J. Comput. Aided Mol. Des. 29 (2015) 249–270.
[20] N.K. Manchukonda, P.K. Naik, B. Sridhar, S. Kantevari, Synthesis and biological evaluation of novel biaryl type α-noscapine congeners, Bioorg. Med. Chem. Lett 24 (2014) 5752–5757.
[21] N.K. Manchukonda, P.K. Naik, S. Santoshi, M. Lopus, S. Joseph, B. Sridhar, S. Kantevari, Rational design, synthesis and biological evaluation of third generation a-noscapine analogues as potent tubulin binding anti-cancer agents, PloS One 8 (2013) e77970.
[22] P.K. Naik, M. Lopus, R. Aneja, S.N. Vangapandu, H.C. Joshi, In silico inspired design and synthesis of a novel tubulin-binding anti-cancer drug: folate conjugated noscapine (Targetin), J. Comput. Aided Mol. Des. 26 (2012) 233–247.
[23] P.K. Naik, B.P. Chatterji, S.N. Vangapandu, R. Aneja, R. Chandra, S. Kanteveri, H. C. Joshi, Rational design, synthesis and biological evaluations of amino-noscapine: a high affinity tubulin-binding noscapinoid, J. Comput. Aided Mol. Des. 25 (2011) 443–454.
[24] H.C. Joshi, Y. Keqiang, J. Kapp, F. Liu, U.S. Patent No. 6,376,516, U.S. Patent and Trademark Office, Washington DC, 2002.
[25] M.A. Oliva, A.E. Prota, J. Rodríguez-Salarichs, Y.L. Bennani, J. Jiménez-Barbero, K. Bargsten, A. Canales, M.O. Steinmetz, J.F. Díaz, Structural basis of noscapine activation for tubulin binding, J. Med. Chem. 63 (2020) 8495–8501.
[26] S. Santoshi, P.K. Naik, Molecular insight of isotypes specific β-tublin interaction of tubulin heterodimer with noscapinoids, J. Comput. Aided Mol. Des. 28 (2014) 751–763.
[27] H.J.C. Berendsen, D. van der Spoel, R. van Drunen, GROMACS: a message passing parallel molecular dynamics implementation, Comput. Phys. Commun. 91 (1995) 43–56.
[28] J. Lehmann, M.H. Wright, S.A. Sieber, Making a long journey short: alkyne functionalization of natural product scaffolds, Chem.–A Euro. J. 22 (2016) 4666–4678.
[29] Y. Wang, G. Schmid-Bindert, C. Zhou, Erlotinib in the treatment of advanced non-small cell lung cancer: an update for clinicians, Thera. Adv. Med. Onc. 4 (2012) 19–29.
[30] G.L. Fekete, L. Fekete, Cutaneous leukocytoclastic vasculitis associated with erlotinib treatment: a case report and review of the literature, Exp. Thera. Med. 17 (2019) 1128–1131.
[31] W. Shi, A. Lei, 1, 3-Diyne chemistry: synthesis and derivations, Tetrahedron Lett. 55 (2014) 2763–2772.
[32] K.Q. Ma, Y.H. Miao, X. Li, Y.Z. Zhou, X.X. Gao, X. Zhang, X.M. Qin, Discovery of 1, 3-diyne compounds as novel and potent antidepressant agents: synthesis, cell-based assay and behavioral studies, RSC Adv. 7 (2017) 16005–16014.
[33] X. Liang, R. Gopalaswamy, I.I.I.F. Navas, E.J. Toone, P. Zhou, A scalable synthesis of the difluoromethyl-allo-threonyl hydroxamate-based LpxC inhibitor LPC-058, T. J. Org. Chem. 81 (2016) 4393–4398.
[34] A.L. Erwin, Antibacterial drug discovery targeting the lipopolysaccharide biosynthetic enzyme LpxC, Col. Spr. Harb. Perspec. Med. 6 (2016) a025304.
[35] C.J. Lee, X. Liang, Q. Wu, J. Najeeb, J. Zhao, R. Gopalaswamy, P. Zhou, Drug design from the cryptic inhibitor envelope, Nat. Commun. 7 (2016) 1–7.
[36] R.R. Gubaidullin, R.R. Khalitova, D.A. Nedopekina, A.Y. Spivak, Homo-and cross coupling of C-2 propargyl substituted triterpenoic acids: synthesis of novel symmetrical and unsymmetrical triterpene 1, 3-diynes, Chem. Sel. 3 (2018) 13526–13529.
[37] O. Sari, V. Roy, J. Balzarini, R. Snoeck, G. Andrei, L.A. Agrofoglio, Synthesis and antiviral evaluation of C5-substituted-(1, 3-diyne)-2′-deoxyuridines, Eur. J. Med. Chem. 53 (2012) 220–228.
[38] P.K. Naik, S. Santoshi, A. Rai, H.C. Joshi, Molecular modelling and competition binding study of Br-noscapine and colchicine provide insight into noscapinoid-tubulin binding site, J. Mol. Graph. Model. 29 (2011) 947–955.
[39] R.A. Friesner, J.L. Banks, R.B. Murphy, T.A. Halgren, J.J. Klicic, D.T. Mainz, M. P. Repasky, E.H. Knoll, M. Shelley, J.K. Perry, D.E. Shaw, P. Francis, P.S. Shenkin, Glide: a new approach for rapid, accurate docking and scoring. 1. Method and assessment of docking accuracy, J. Med. Chem. 47 (2004) 1739–1749.
[40] T.A. Halgren, R.B. Murphy, R.A. Friesner, H.S. Beard, L.L. Frye, W.T. Pollard, J. L. Banks, Glide: a new approach for rapid, accurate docking and scoring. 2. Enrichment factors in database screening, J. Med. Chem. 47 (2004) 1750–1759.
[41] R. Zhou, R.A. Frienser, A. Ghosh, R.C. Rizzo, W.L. Jorgensen, R.M. Levy, New linear interaction method for binding affinity calculations using a continuum solvent model, J. Phys. Chem. B 105 (2001) 10388–10397.
[42] S. Santoshi, P.K. Naik, H.C. Joshi, Rational design of novel anti-microtubule agent (9-azido-Noscapine) from quantitative structure activity relationship (QSAR) evaluation of noscapinoids, J. Biomol. Screen 16 (2011) 1047–1058.
[43] N.K. Manchukonda, B. Sridhar, P.K. Naik, H.C. Joshi, S. Kantevari, Copper (I) mediated facile synthesis of potent tubulin polymerization inhibitor, 9-amino-α-noscapine from natural α-noscapine, Bioorg. Med. Chem. Lett 22 (2012) 2983–2987.
[44] R. Aneja, S.N. Vangapandu, M. Lopus, V.G. Viswesarappa, N. Dhiman, A. Verma, R. Chandra, D. Panda, H.C. Joshi, Synthesis of microtubule-interfering halogenated noscapine analogues that perturb mitosis in cancer cells followed by cell death, Biochem. Pharmacol. 72 (2006) 415–426.
[45] N. Jain, D. Yada, T.B. Shaik, G. Vasantha, P.S. Reddy, S.V. Kalivendi, B. Sreedhar, Synthesis and antitumor evaluation of nitrovinyl biphenyls: anticancer agents based on allocolchicines, ChemMedChem 6 (2011) 859–868.